International Journal of Pharmaceutics 361 (2008) 141–149

Contents lists available at ScienceDirect

International Journal of Pharmaceutics

journal homepage: www.elsevier.com/locate/ijpharm

Polymorphic control of inhalation microparticles prepared by crystallization

Darragh Murnane, Christopher Marriott, Gary P. Martin*

King's College London, Drug Delivery Research Group, Pharmaceutical Science Division, 150 Stamford Street, London SE1 9NH, United Kingdom

ARTICLE INFO

Article history:
Received 11 February 2008
Received in revised form 9 May 2008
Accepted 23 May 2008
Available online 4 June 2008

Keywords:
Inhalation
Aerosol
Antisolvent micronization
Polymorphism
Salmeterol xinafoate
Differential scanning calorimetry
Thermal kinetic analysis

ABSTRACT

Milling processes are known to cause polymorphic transition in enantiotropic systems and the micronization process employed to produce microparticles for inhalation formulations has been reported to result in solid-state damage. The aim of the current work was to investigate the polymorphism of salmeterol xinafoate (SX) following antisolvent micronization from poly(ethylene glycol) (PEG) solvents and compare this to the properties of SX conventionally crystallized and micronized. Powder X-ray diffraction revealed that SX crystallized predominantly as the SX form I polymorph following rapid precipitation from PEG solvents and cooling crystallization from propan-2-ol. Thermo-kinetic analysis using a modified Avrami–Erofe'ev equation was applied to differential scanning calorimetric thermographs of crystallized and micronized SX. The kinetic analysis revealed that SX crystallized from PEG solvents underwent significantly less or no re-crystallization of SX form II from the melt. A polymorphic transition was identified upon heating ball-milled SX, although the untreated material was resistant to such transformation. The thermal behaviour of SX crystallized from PEG solvents was consistent with a lower degree of crystal lattice disorder and higher enantiotropic purity than SX crystallized from propan-2-ol; the same was also true when comparing SX before and after micronization.

1. Introduction

Salmeterol xinafoate (SX) (4-hydroxy-α[1]-[[[6-(4-phenylbutoxy)hexyl]amino]methyl]1,3-benzenedimethanol, 1-hydroxy-2-napthoate) is a long-acting bronchodilator used in the treatment of asthma and COPD (Chung and O'Byrne, 2003). The production of SX for inhalation formulations is typical of the current technology where the API is produced by batch crystallization from a suitable solvent followed by micronization (jet-milling) to produce particles in the appropriate size range for topical therapy of obstructive lung diseases (2.5–6 μm; Pritchard, 2001). The process employed for producing SX involves the drug substance being crystallized from a hot solution of propan-2-ol by the quench cooling that results after addition to cooled propan-2-ol (Beach et al., 1999). Crystallization in this manner results in spherically agglomerated macrocrystals which are more suitable for micronization.

SX exhibits enantiotropic polymorphism (Tong et al., 2001). In enantiotropy a definitive transition point exists because the free energy difference between the polymorphs decreases as a function of temperature, allowing the inter-conversion of polymorphic forms in a solid-state transformation. Any mechanism that introduces energy into the system (e.g. mechanical or tribomechanical) can induce a spontaneous and reversible transformation between polymorphs in enantiotropes (Zhang et al., 2004), although a kinetic barrier may prevent its occurrence (Morris et al., 2001). Grinding and milling are obviously a critical concern for particles for inhalation due to the necessity for size reduction to the respirable size range. Micronization is a high-energy process that introduces amorphous character into drug particles (i.e. a metastable phase) (Elamin et al., 1994; Ward and Schultz, 1995; Mackin et al., 2002b; Steckel et al., 2003). The surface energy of a number of pharmaceuticals is increased by milling (York et al., 1998; Planinsek and Buckton, 2003; Heng et al., 2006). In the particular case of SX, the micronized material and the metastable polymorph at room temperature (SX II) have a higher surface energy than the stable polymorph SX I. Surface energy affects the flow properties (Rehman et al., 2004), blending homogeneity (Mackin et al., 2002a) and efficiency of aerosolization of micronized particles (Tong et al., 2006).

An investigation into the polymorphism of SX has revealed the existence of an enantiotropic pair SX I (characterized by a melting point at ~125 °C) and SX II (characterized by a melting point at ~139 °C) (Beach et al., 1999). Commercial pre-micronized granular SX (gSX) and the micronized SX (mSX) materials are predominantly the stable form I polymorph (Shekunov et al., 2002; Tong et al., 2003) but SX II recrystallizes exothermically in both following melting of SX I. The relative stability transition point for the SX I–SX II pair has been estimated to be between 80 °C (Beach et al., 1999) and 99–110 °C (Tong et al., 2001), admittedly a large range. Poly-

* Corresponding author. Tel.: +44 20 7848 4791; fax: +44 20 7848 4800.
E-mail address: gary.martin@kcl.ac.uk (G.P. Martin).

0378-5173/$ – see front matter © 2008 Elsevier B.V. All rights reserved.
doi:10.1016/j.ijpharm.2008.05.033

morphically pure SX I produced by Solution Enhanced Dispersion by Supercritical fluid (SEDS™) antisolvent crystallization (Beach et al., 1999; Shekunov and York, 2000) displayed a much reduced conversion to SX II from the melt than either commercial gSX or mSX (Tong et al., 2001), but nevertheless did display re-crystallization. The greater conversion of SX in gSX and mSX from SX form I to the form II polymorph upon heating has been attributed to the presence of disorder in the crystal lattice (Shekunov et al., 2002), or the presence of small quantities of SX II seeds in the SX I crystal lattice (Tong et al., 2003).

It has been suggested that aggressive quench crystallization of SX leads to crystal disorder of the SX I lattice (Shekunov et al., 2002), which is then increased by the milling process. An environmentally benign aqueous antisolvent crystallization process, termed Amphiphilic Crystallization, has been developed recently for the production of microparticles of APIs (including SX) for inhalation (Murnane et al., 2008a). The aim of the current work was to investigate the crystallinity and polymorphic form of SX microparticles produced according to this process and to compare these to the properties of SX crystallized using organic solvents. The effects of sample micronization and milling were also to be examined with a view to investigating further the enantiotropic polymorphism of SX by employing a thermokinetic analytical approach.

2. Materials and methods

2.1. Chemicals and reagents

PEG 400, Analar® grade cyclohexane and HiPerSolv® grade ammonium acetate were purchased from BDH (VWR International Ltd., Poole, UK). High-performance liquid chromatography grade methanol and reagent grade propan-2-ol was purchased from Fisher Scientific Ltd. (Loughborough, UK) or from VWR International Ltd. (Poole, UK). PEG 6000 (Fluka Biochemika Ultra grade) and Span 80 was purchased from Sigma–Aldrich Company Ltd. (Gillingham, UK). Nylon filters (0.45 μm pore size, 47 mm diameter) and cellulose acetate syringe filters (0.45 μm pore size, Schleicher and Schuell brand) were obtained from Whatman Intl. Ltd. (Maidstone, UK). Water was produced by reverse osmosis using an ElgaStat unit (Elga LabWater, Marlow, UK). Silica gel was purchased from Prolabo (VWR International Ltd., Poole, UK). Salmeterol xinafoate was a generous gift from GlaxoSmithKline Pharmaceutical Development (Ware, UK).

2.2. Crystallization of salmeterol xinafoate

2.2.1. Production of SX microparticles

SX particles were produced by Amphiphilic Crystallization from solutions of 4% (w/w) SX in PEG 400 (SX PEG 400) and in PEG 6000 (SX PEG 6000) by the addition of water to the drug solutions (SX PEG 400 = 14.0 g and SX PEG 6000 = 14.3 g). The drug solution to antisolvent ratio (w:w) employed was 1:11 and water was added to the drug solution at an addition rate of 350 g min^{-1} with stirring at 1100 rpm (SX PEG 400A) and 650 rpm (SX PEG 6000). The crystals were harvested according to the previously developed protocol (Murnane et al., 2008b). A further solution of 4.5% (w/w) SX in PEG 400 (28.9 g) was crystallized by the addition of water at a drug solution to antisolvent ratio of 1:16 at an addition rate 200 g min^{-1} and a stirring rate of 550 rpm (SX PEG 400B).

The dried powders were washed once more with 200 mL of filtered SX-saturated water at a temperature of 4 °C by stirring continuously in a 250 mL glass beaker for 5 min. The water had been saturated with SX by stirring overnight with SX raw material and then cooled in a refrigerator. The washed drug crystals were recovered by filtration (0.45 μm nylon filters) and the filter cakes were washed on the filter with 100 mL of unsaturated filtered cold water. These washed crystals were dried *in vacuo* overnight at 50 °C. The dried cakes were transferred to sealable glass vials and 15 mL of cyclohexane (BDH Ltd-VWR International, UK) was added to each. The vials containing the suspensions of SX in cyclohexane were sonicated for 6 min in a Decon FS300B bath (Decon Laboratories Ltd., UK) to break up the filter cake. The cyclohexane was removed by heating the vials in the vacuum oven at 50 °C overnight. The de-caked crystals were stored over silica gel in sealed glass vials at room temperature.

2.2.2. Production of SX macrocrystals

A 1.6% (w/v) suspension of SX in propan-2-ol (110 mL) was prepared in a 250 mL round bottom flask and purged with nitrogen gas. The suspension was heated at 60 °C on an oil bath placed on a magnetic stirrer hot plate. The solution was left to stir gently for 30 min to achieve dissolution of the SX. Crystallization was achieved by cooling with gentle stirring to 45 °C over 2 h, followed by natural cooling to 37 °C, at which temperature the suspension was aged overnight. The suspension was then allowed to cool to 25 °C, at which temperature the crystalline suspension was allowed to age once more overnight, before finally being cooled to 21 °C, at which stage the crystals were harvested by filtration and dried in a vacuum oven overnight at 50 °C. The crystals were washed using 100 mL of SX-saturated propan-2-ol (4 °C) in place of water.

2.3. Particle size analysis

SX particle size was determined by laser diffraction using a Malvern Mastersizer X (Malvern Instruments Ltd, Malvern, UK) equipped with a 100 mm lens validated according to ISO 13320 (1990) standards. The dispersant liquid was an SX-saturated solution of 0.5 % w/v Span 80 in cyclohexane.

2.4. Investigations into the polymorphism of salmeterol xinafoate particles

2.4.1. Milling of SX

SX particles (macrocrystals and SX PEG 6000) were milled in a Retsch MM200 ball mill (Glen Creston Ltd., Stanmore, UK) using zirconium oxide 25 mL grinding jars. Powder (~150 mg of SX PEG 6000 and ~500 mg SX macrocrystals) was filled into the grinding jar along with 10 stainless steel beads (diameter = 1/8″) (Malvern Instruments, Malvern, UK). Milling was achieved by oscillation at 30 s^{-1} for 30 min. Milled powder was stored in sealed glass vials over phosphorous pentoxide at −15 °C.

2.4.2. Powder X-ray diffraction

Powder X-ray diffraction was performed on SX particles using a Philips PW 1730 X-ray diffractometer system (Philips Analytical, UK). X-rays were generated by a PW1730 4 kW X-ray generator operated at 40 kV tension and with a current of 25 mA using a PW2273/30 copper anode (Cu Kα source, λ = 1.5148 Å). Samples were prepared by back-filling a sample mount consisting of an aluminium frame placed over a glass microscope slide. Samples were scanned from $2\theta = 4°$ to 30°, with a step size of 0.04° and a count time of 2 s per step, using a PW1820 goniometer. Detection was by means of a PW1710 xenon detector.

2.4.3. Differential scanning calorimetry

Thermographs were produced using a TA 2920 modulated differential scanning calorimeter (TA Instruments, UK). Approximately 1–2 mg of the test material was weighed accurately into 40 μL aluminum pans (TA Instruments, UK). Hermetically sealed

Table 1
Particle size distribution of salmeterol xinafoate particles (mean ± SD, n = 5)

Experiment	$D_{(v,0.1)}$ (μm)	$D_{(v,0.5)}$ (μm)	$D_{(v,0.9)}$ (μm)
Micronized SX	0.59 ± 0.01	1.13 ± 0.12	3.69 ± 0.23
SX PEG 6000	0.59 ± 0.01	1.23 ± 0.06	8.72 ± 0.22
SX PEG 400A	0.67 ± 0.01	3.66 ± 0.22	10.78 ± 0.51
SX PEG 400B	1.06 ± 0.06	6.59 ± 0.31	14.55 ± 0.63
Macrocrystalline SX	3.44 ± 0.11	11.43 ± 0.21	23.52 ± 0.64
Milled macrocrystalline SX	0.74 ± 0.02	5.10 ± 0.41	25.90 ± 0.71

pans were employed for both reference and sample pans. The instrument was calibrated according to the manufacturer's instructions for each heating rate using an indium standard. Samples were heated from 30 to 160 °C at the following heating rates: 2, 5, 10, 20, 40 and 70 °C min^{-1}. Transition temperatures were taken as the point of intersection between the extrapolated baseline before the onset of transition, and the extrapolated down slope of the transition peak. Enthalpies of transitions were derived by integration of the relevant peak.

2.4.4. Hot stage microscopy

Samples of salmeterol xinafoate were heated at a rate of 10 °C min^{-1} from 30 to 140 °C using an FP 82 hot stage module (Mettler Toledo, UK) mounted on a Leica DME long distance objective microscope with cross polarizing lens (Leica Microsystems, Germany) and an FP 90 thermal controller module (Mettler-Toledo, UK).

3. Results

3.1. Particle size distribution

The particle size distribution of SX microparticles was measured as previously reported (Murnane et al., 2008b) by laser diffraction analysis are presented in Table 1. The process of secondary washing and de-caking the particles in cyclohexane was demonstrated not to have any effect on the particle size distribution of SX PEG microparticles (data not presented; Student's *t*-test $p > 0.190$).

3.2. Polymorphism of salmeterol xinafoate particles

The X-ray diffraction pattern of the starting material, i.e. micronized SX, is presented in Fig. 1, with the patterns obtained from two reference samples of SX; polymorphic forms I and II (kindly donated by Prof. Peter York, University of Bradford). Fig. 1 clearly illustrates the different diffraction angles for SX polymorphs II and I and that mSX presents as the form I polymorph. The X-ray

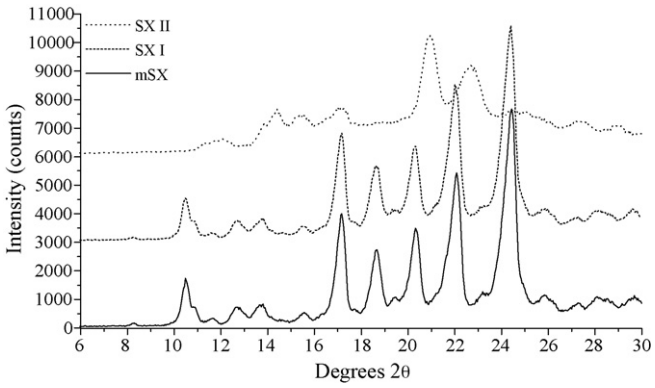

Fig. 1. Comparative powder X-ray diffractogram of salmeterol xinafoate polymorph I (SX I), polymorph II (SX II) and the commercial micronized material (mSX).

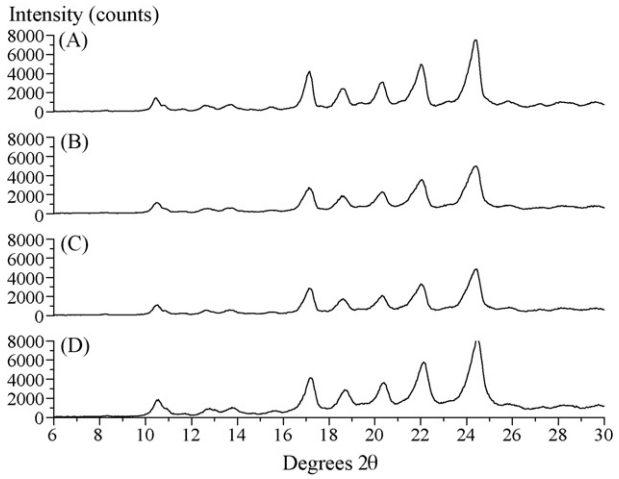

Fig. 2. Comparative powder X-ray diffractogram of salmeterol xinafoate microparticles produced by antisolvent crystallization from PEG 400 and PEG 6000 by the addition or water ((A) SX PEG 400B, (B) SX PEG 400A and (C) SX PEG 6000) and by cooling crystallization in propan-2-ol (D).

diffraction profiles of the SX microparticles crystallized from PEG solvents are presented in Fig. 2, along with that obtained for SX crystallized from propan-2-ol. Comparison of the diffraction profiles with those of Fig. 1 indicated that SX presents as the form I polymorph in all cases for the SX material crystallized in the current study. The peak positions (2θ) and the integral breadth values ($\beta^{\bullet\bullet}$) are presented in Table 2 for each of six diffraction angles characteristic of SX form I.

PXRD is conventionally applied to determine the crystallinity of sample powders based on the line broadening, peak intensity and background. All samples demonstrated a high background, which contributed to the difficulty in using PXRD to verify the absence of crystallinity on the basis of peak intensities. Nevertheless, mSX and SX crystallized from isopropanol displayed similar peak heights, which were higher than those of SX microcrystals produced from PEG solvents. A high background arises from difficulties in preparing samples of crystals of small size and preferred orientation affects (Giacovazzo, 1996), which can be confused with the presence of amorphous regions. No significant differences in the integral breadths were observed between any of the SX materials (ANOVA, $p > 0.081$), which indicated similar levels of lattice strain. However, the presence of crystals below 5 μm also introduces line broadening (Langford and Louer, 1996). The differences in proportions of crystals below 5 μm between the samples renders conclusive comparison of line broadening due to lattice strain difficult.

When samples of SX PEG 6000 and macrocrystalline SX were subjected to mechanical comminution (ball milling), an underlying halo effect was generated (Figs. 3 and 4). The peaks also appeared broader and/or of lower intensity following milling. Certain fine structure of the diffraction pattern was lost after milling; e.g. the shoulder at 10.5° and peaks at 15.5° and 26° 2θ. The qualitative change in the X-ray diffraction pattern after milling was most apparent for SX PEG 6000, although no statistical difference in broadening of the integral breadths (Student's *t*-test, $p > 0.05$) was observed between the starting material and the milled powder (Table 2), presumably because only duplicate measurements were made on the milled material. The similar peak intensities before and after milling of SX crystallized from isopropanol as well as the low degree of peak broadening (Fig. 4) may have arisen due to the significant population of particles which were not milled effectively (see $D_{(v,0.9)}$ values in Table 1). The generation of a halo effect and peak

Table 2
The position (2θ) and integral breadth ($\beta^{\bullet\bullet}$) of characteristic diffraction peaks of the salmeterol xinafoate particles (mean ± S.D., $n = 3$, except $^{*}n = 2$)

	2θ (°)	$\beta^{\bullet\bullet}$ (°)
Macrocrystalline SX	15.5 ± 0.07	0.46 ± 0.03
	17.2 ± 0.02	0.55 ± 0.06
	18.7 ± 0.05	0.52 ± 0.02
	20.4 ± 0.02	0.50 ± 0.04
	22.1 ± 0.04	0.64 ± 0.04
	24.4 ± 0.02	0.73 ± 0.06
Milled macrocrystalline SX	15.6 ± 0.06	0.42 ± 0.03
	17.2 ± 0.05	0.52 ± 0.06
	18.7 ± 0.02	0.51 ± 0.03
	20.4 ± 0.02	0.50 ± 0.02
	22.1 ± 0.02	0.60 ± 0.04
	24.5 ± 0.06	0.67 ± 0.08
SX reference form I	15.5 ± 0.12	0.46 ± 0.04
	17.2 ± 0.06	0.53 ± 0.01
	18.7 ± 0.06	0.52 ± 0.02
	20.4 ± 0.07	0.53 ± 0.04
	22.1 ± 0.06	0.62 ± 0.03
	24.4 ± 0.02	0.71 ± 0.05
SX PEG 400A	15.5 ± 0.08	0.43 ± 0.02
	17.1 ± 0.02	0.55 ± 0.01
	18.6 ± 0.05	0.53 ± 0.01
	20.3 ± 0.00	0.51 ± 0.01
	22.1 ± 0.02	0.67 ± 0.01
	24.4 ± 0.02	0.76 ± 0.03
SX PEG 6000	15.5 ± 0.04	0.42 ± 0.02
	17.2 ± 0.02	0.57 ± 0.01
	18.7 ± 0.02	0.54 ± 0.02
	20.3 ± 0.04	0.51 ± 0.02
	22.0 ± 0.04	0.66 ± 0.02
	24.4 ± 0.02	0.76 ± 0.01
Milled SX PEG 6000*	15.4 ± 0.00	0.36 ± 0.00
	17.0 ± 0.06	0.62 ± 0.02
	18.5 ± 0.06	0.52 ± 0.00
	20.2 ± 0.11	0.54 ± 0.02
	21.9 ± 0.03	0.78 ± 0.03
	24.3 ± 0.03	0.76 ± 0.01
SX PEG 400B	15.5 ± 0.08	0.45 ± 0.02
	17.2 ± 0.04	0.54 ± 0.01
	18.6 ± 0.02	0.53 ± 0.02
	20.3 ± 0.02	0.52 ± 0.02
	22.0 ± 0.05	0.66 ± 0.01
	24.4 ± 0.02	0.75 ± 0.02
Micronized SX	15.5 ± 0.05	0.40 ± 0.03
	17.2 ± 0.02	0.52 ± 0.01
	18.7 ± 0.04	0.49 ± 0.02
	20.3 ± 0.02	0.48 ± 0.01
	22.1 ± 0.02	0.61 ± 0.02
	24.4 ± 0.04	0.66 ± 0.06

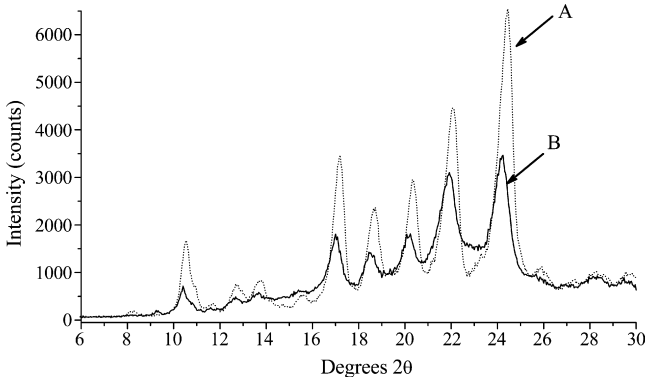

Fig. 3. Powder X-ray diffractogram of SX PEG 6000 (A) before and (B) after mechanical processing.

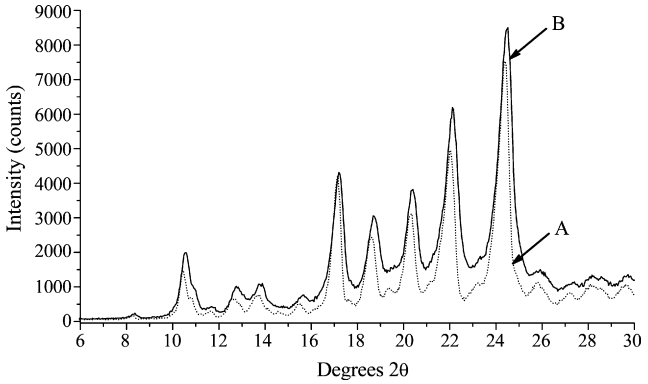

Fig. 4. Powder X-ray diffractogram of salmeterol xinafoate crystallized by cooling in propan-2-ol (A) before and (B) after mechanical processing.

broadening are symbolic of the generation of amorphous character and lattice disorder in a crystalline material, respectively (Shah et al., 2006). Peak broadening has been observed using higher resolution synchrotron PXRD for SX following micronization (Shekunov et al., 2002).

3.3. Thermal behaviour of SX particles

Fig. 5 demonstrates the melting and re-crystallization behaviour of the standard SX form I, SX form II, commercial micronized SX material and macrocrystalline SX employing a heating rate of 2 °C min^{-1}. SX form I melts at ~121 °C, followed by an exotherm corresponding to re-crystallization of SX II from the melt. SX form II melts at ~137 °C. Fig. 6 demonstrates the melting behaviour of SX crystallized from PEG solvents at the same heating rate. SX material re-crystallized from PEG solvents either underwent no (SX PEG 400A and SX PEG 6000) or significantly lower (SX PEG 400B) conversion to the SX II polymorph upon heating in comparison to SX form I, mSX or macrocrystalline SX. At this low heating rate, significant conversion to SX II was expected, as shown by the reference standard SEDS SX I. Hot stage microscopy revealed that re-crystallization of SX II in the case of mSX was isolated to droplets of the melt where solid seeds were observed (Fig. 7). Such re-crystallization was confirmed to be absent following melting of SX crystallized from PEG 6000.

The crystallization of SX II from the melt was inhibited in all cases by increasing the heating rate to 40 °C min^{-1}. An example of this behaviour is presented for macrocrystalline SX in Fig. 8. A melting endotherm corresponding to that of SX II was observed at low heating rates for SX PEG 400B crystals. The resultant endotherm was, however, of lower intensity than that obtained for the SX form I, mSX or macrocrystalline SX and no re-crystallization exotherm could be discerned. Additionally, the SX II endotherm was suppressed at lower heating rates (20 °C min^{-1}) than for SX I, macrocrystalline SX and mSX.

No differences were found between the enthalpy of fusion of SX form I for SX PEG 6000 (62.36 ± 2.91 kJ mol^{-1}), SX PEG 400A (63.89 ± 3.13 kJ mol^{-1}) and SX PEG 400B (65.69 ± 1.46 kJ mol^{-1}) when the heating rate was varied (ANOVA, $p > 0.08$, $n = 3$). The enthalpies of fusion of the SX I polymorph of the remaining samples were determined at the heating rate, which prevented the re-crystallization of SX form II. The highest enthalpy was seen for macrocrystalline SX (73.84 ± 2.25 kJ mol^{-1}), but no significant difference was found between the values obtained and those determined for the milled macrocrystalline material (68.42 ± 4.82 kJ mol^{-1}) or commercial mSX (68.49 ± 2.12 kJ mol^{-1}) (Tukey's test, $p < 0.05$). Additionally no significant difference was

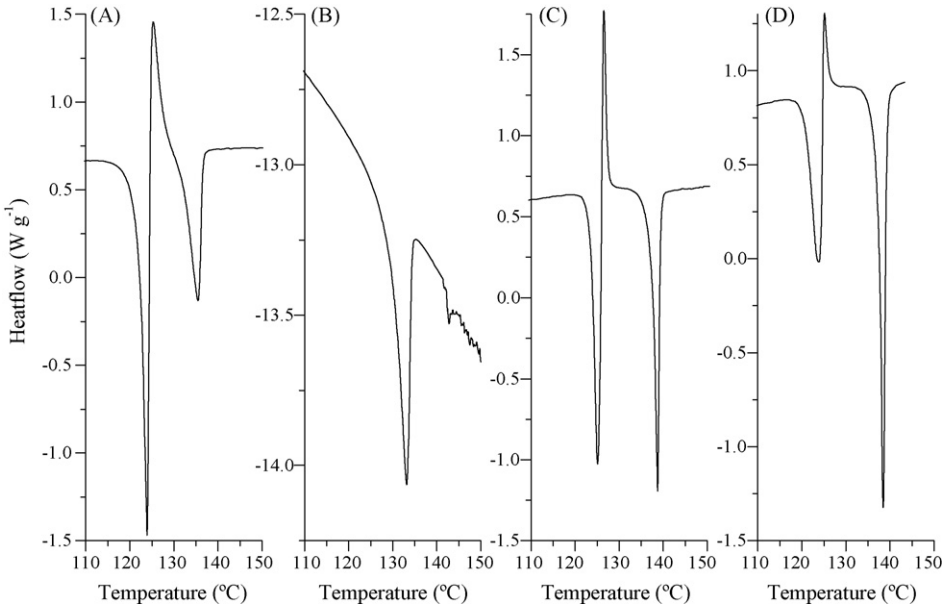

Fig. 5. Differential scanning calorimetry thermographs at heating rate of 2 °C min^{-1} of SX particles: (A) SEDS SX form I; (B) SEDS SX form II; (C) SX crystallized by cooling in propan-2-ol; (D) commercial micronized SX.

demonstrated in the enthalpy of fusion of mSX, reference standard SX I (65.65 ± 1.29 kJ mol^{-1}), SX PEG 6000, SX PEG 400A and the milled macrocrystalline material.

3.4. Thermo-kinetic analysis of SX enantiotropism

3.4.1. Theoretical basis for analysis

The kinetic profile of the re-crystallization process was studied by constructing an α-heating rate (β, °C min^{-1}) curve, where α, the fraction re-crystallized from the melt, is given by the following equation:

$$\alpha = \frac{\Delta H_f^{\beta\,\mathrm{exp}}}{\Delta H_f^{\mathrm{ref}}} \quad (1)$$

where $\Delta H_f^{\beta\,\mathrm{exp}}$ is the enthalpy of fusion of SX II determined by experiment at the particular heating rate and $\Delta H_f^{\mathrm{ref}}$ is the standard literature value of the enthalpy of fusion of SX II (42.02 kJ mol^{-1}; Tong et al., 2001).

An Avrami–Erofe'ev-type Equation (2) was fitted to the data to generate the kinetic parameters k and n, where k is an integrated rate constant for the re-crystallization of SX II, and n is the Avrami exponent of the model (Michaelsen and Dahms, 1996). Fitting was performed using the Levenberg–Marquardt algorithm of a non-linear least squares fitting programme in Origin 7.5 (OriginLab, USA). Due to the variance in the data, individual data points were plotted.

$$\alpha = 1 - \exp^{-(k\beta^{-1})^n} \quad (2)$$

The AE equation is generally applied to α-time curves rather than α-heating rate curves when explaining the condensation of a crystallite from the melt (Kaschiev, 2000). A sigmoidal plot of conversion as a function of time is observed as a result of nucleation,

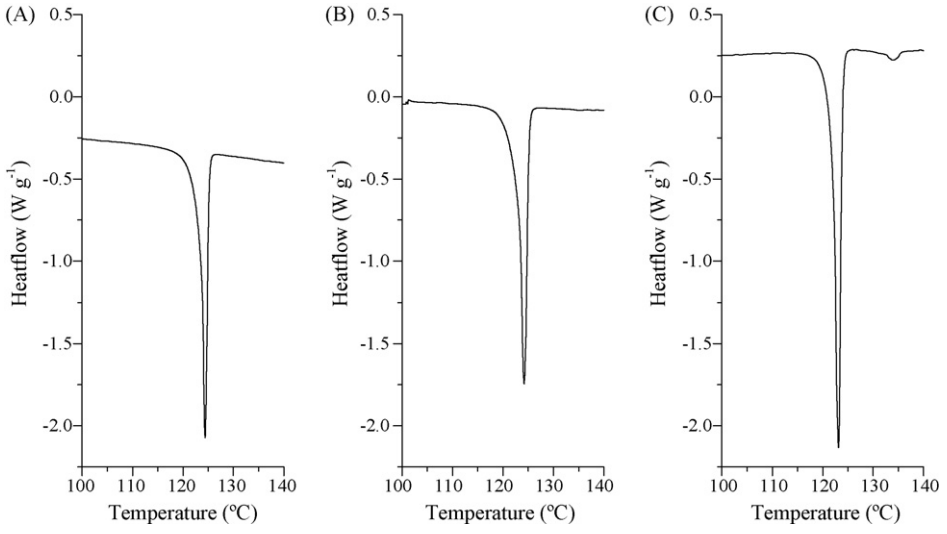

Fig. 6. Differential scanning calorimetry thermographs at heating rate of 2 °C min^{-1} of SX microparticles produced by Amphiphilic Crystallization: (A) SX PEG 400A; (B) SX PEG 6000; (C) SX PEG 400B.

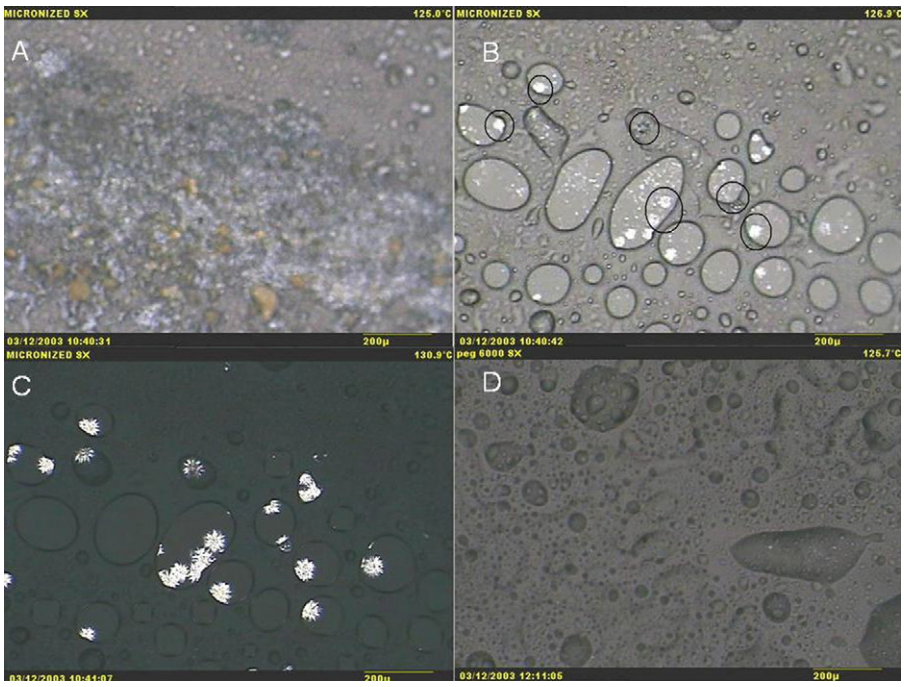

Fig. 7. Hot stage micrographs of mSX taken at (A) 125.0 °C; (B) 126.9 °C; (C) 130.9 °C; (D) of SX PEG 6000 at 126.7 °C.

nucleus growth and finally impingement of nuclei in cases of both homogeneous and heterogeneous nucleation (Avrami, 1939, 1940, 1941). The AE equation, however, was derived only for isothermal conditions (Michaelsen and Dahms, 1996). In the case of dynamic heating experiments, the AE equation cannot be applied, because the rate constant of the process changes as a function of temperature (Avrami, 1940; Zhou et al., 2003) and the integrated rate Eq. (3) takes the form (Vyazovkin and Wight, 1997)

$$g(\alpha) = \frac{A}{\beta}\int_0^T \exp\left(\frac{-E}{RT}\right) \mathrm{d}T \tag{3}$$

where E and A are the Arrhenius activation energy and pre-exponential factors, β is the heating rate, R is the universal gas constant and T is the temperature. It is clear that the conversion factor is therefore a function of temperature and cannot be separated from the change in time ($\beta = \mathrm{d}T/\mathrm{d}t$). The inability to separate the rate of crystallization from the rate of heating upon integration was shown in a modified form of the AE equation for solid-state changes not involving melts as (4) (Vazquez et al., 2000)

$$\alpha(t) = 1 - \exp\left[-\left(\int_0^t K[T(t')\mathrm{d}t']\right)^n\right] \tag{4}$$

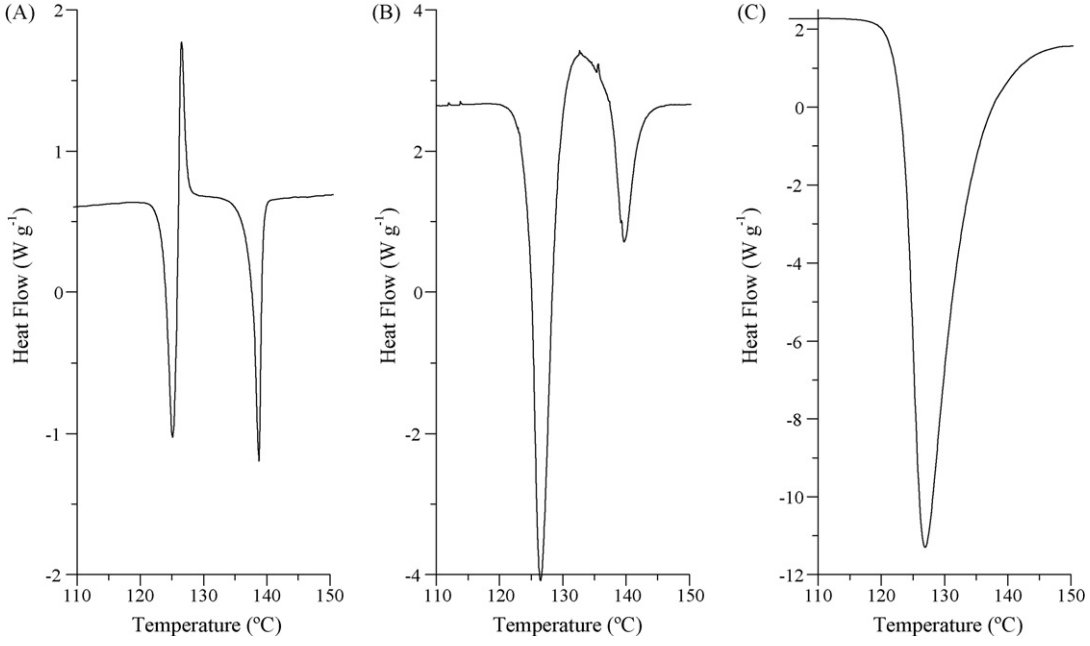

Fig. 8. Differential scanning calorimetry thermographs of SX crystallized by cooling in propan-2-ol at heating rate of (A) 2 °C min^{-1}, (B) 10 °C min^{-1} and (C) 40 °C min^{-1}.

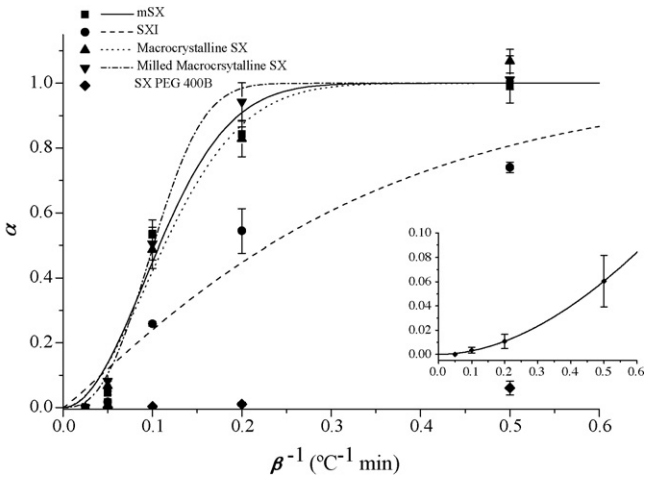

Fig. 9. α-Heating rate curves displaying the degree of re-crystallization of salmeterol xinafoate form II polymorph from the melt (α) as a function of the heating rate (β^{-1}) for mSX; SEDS SX I; SX crystallized by cooling in propan-2-ol before and after mechanical processing and SX PEG 400B (the inset represents the plot of SX PEG 400B on an enlarged scale).

The integral function of $K[T(t')]$ represents the sum of the instantaneous reaction rate constants at every time, t', earlier than time, t, at which a particular value of α is determined and n is the kinetic exponent.

Although non-isothermal (dynamic) methods may be applied for analysis of solid-state transitions upon heating, the situation is complicated by the concomitant melting and re-crystallization events, such that the enthalpy response is not separated for either event. It is for this reason that in the current non-isothermal study the conversion plots were constructed as α as a function of β instead of t. In particular Eq. (2) was derived because $g(\alpha)$ is proportional to β^{-1} (see Eq. (3)). Such an approach does not apply a false interpretation to the definitions of k and n as AE kinetic parameters.

3.4.2. Experimental observation

The α–β curves for the materials which underwent re-crystallization (i.e. excluding SX PEG 400A and SX PEG 6000) are presented in Fig. 9. The plot shows the mean values of α, whereas the kinetic parameters were obtained by fitting all data points; and the regression analyses are presented in Table 3. The k values demonstrated there was no significant difference between the degree (rate) of re-crystallization of mSX, macrocrystalline SX and milled macrocrystalline SX material, as the three k values all fell within their respective 95% confidence intervals of determination. Re-crystallization of SEDS SX I was significantly slower than the above three materials, while SX PEG 400B underwent a significantly lower conversion than any of the other four materials.

The 'goodness of fit' was judged by the magnitude of the errors in conjunction with the coefficient of determination (R^2). It is not appropriate to consider the coefficient of determination alone to assess the quality of a linear fitting process (Sonnergaard, 2006), without a consideration of the contribution of the parameter errors. From Table 3 it can be seen that the R^2 values were greater than 0.86 and the error in determining k values was less than 13.4% (excluding SX PEG 400B). This corresponded to an adequate model fit for all materials excluding SX PEG 400B. The study of more heating rates would enable improvement of the fitting process. The AE model fitted the SX PEG 400B data more poorly with higher errors in comparison to the other samples. This was presumably due to the low fractions converted over the time course studied.

3.4.2.1. Solid-state transition of salmeterol xinafoate enantiotropes. A solid-state transition from SX I to SX II was observed in the processed SX PEG 6000 material at heating rates of 2 °C min^{-1} (Fig. 10) and 5 °C min^{-1} (data not shown) where the melting endotherm of SX I was absent and a new endotherm was observed at 111.1 ± 1.3 °C (n = 6) followed by SX II melting (133.9 ± 1.5 °C (n = 6)). The mean enthalpy of this endotherm obtained at these two slowest heating rates was calculated to be 26.58 ± 1.66 kJ mol^{-1} (n = 6), which is approximately equivalent to the differences in the enthalpies of fusion of SX I and SX II. No re-crystallization exotherm of SX II was observed until higher heating rates (≥10 °C min^{-1}) were employed. A heating rate to 20 °C min^{-1} was surprisingly associated with an increase in the intensity of the re-crystallization exotherm. A summary of the thermal behaviour at various heating rates is presented in Table 4. No significant difference was determined for milled SX PEG 6000 between the ΔH_f of SX II (ANOVA, p = 0.743) at 2, 5, 10 and 20 °C min^{-1}. The ΔH_f at 70 °C min^{-1} was significantly lower than at any of the lower heating rates (p < 0.05).

4. Discussion

In all cases, the crystallization of SX, whether by cooling crystallization in propan-2-ol or antisolvent crystallization from PEG solvents resulted in SX crystalline material of the form I polymorph. The isolation of SX as the form I polymorph has been reported previously regardless of whether a rapid quench crystallization or a slower batch cooling crystallization process was effected (Tong et al., 2001) and regardless of whether seeds of the form II polymorph were introduced during nucleation (Beach et al., 1999).

All crystallization processes were performed at a temperature below the identified transition temperature range of 80–100 °C. The most thermodynamically stable polymorph according to a free energy–temperature plot (Burger and Ramberger, 1979) is there-

Table 3
Non-linear regression analysis of the α-heating rate curves for the re-crystallization of salmeterol xinafoate from the melt fitted by the Avrami–Erofe'ev-type rate Equation (2)

Material	Parameter	Value	S.E.	Error (%)	95% CI	R^2
mSX	k (°C^{-1} min)	7.727	0.413	5.342	0.892	0.9719
	n	2.009	0.241	12.002	0.521	
SX I	k (°C^{-1} min)	3.128	0.293	9.355	0.632	0.9273
	n	1.113	0.132	11.902	0.286	
Macrocrystalline SX	k (°C^{-1} min)	8.219	1.103	13.416	2.382	0.8649
	n	1.462	0.353	24.116	0.762	
Milled macrocrystalline SX	k (°C^{-1} min)	8.608	0.323	3.753	0.698	0.9885
	n	2.626	0.337	12.817	0.727	
SX PEG 400B	k (°C^{-1} min)	0.465	0.186	40.041	0.410	0.8829
	n	1.902	0.511	26.857	1.125	

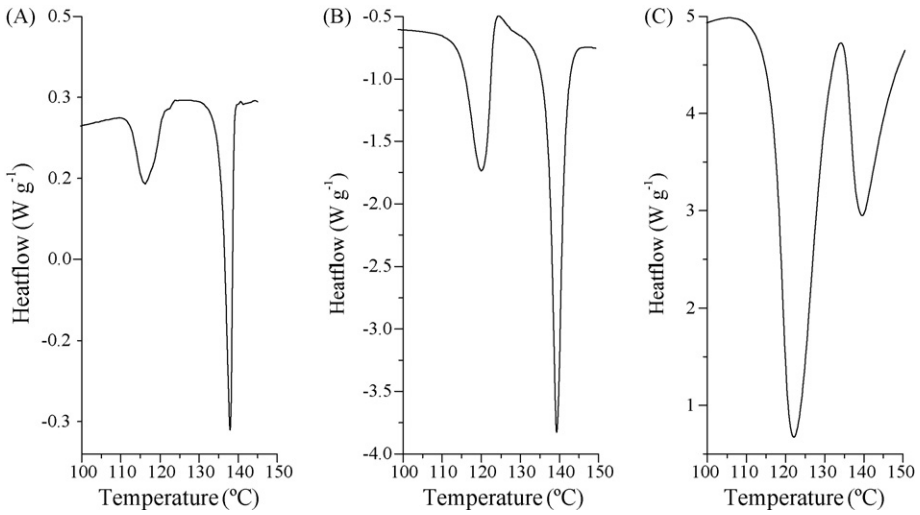

Fig. 10. Differential scanning thermographs of SX PEG 6000 following milling at a heating rate of (A) 2 °C min^{-1}, (B) 10 °C min^{-1} and (C) 70 °C min^{-1}.

fore the form I polymorph. Ostwald's rule of stages states that the metastable polymorph (SX II in this instance) should, in fact, crystallize initially from a supersaturated solution (Blagden and Davey, 2003). Whether Ostwald's rule is followed depends on the stability of a nascent polymorphic nucleus as well as the kinetic rate of nucleation (ter Horst et al., 2002). The nucleation rate can be expressed as

$$J = \nu n_1 \exp\left(-\frac{fV^2\gamma^3}{kT(\Delta\mu)^2}\right) \quad (5)$$

where J is the nucleation rate, ν is a frequency pre-exponential factor, n_1 is the solute concentration, f is a geometrical factor of the nucleus, V is the molecular volume, γ is the interfacial energy, k is the Boltzmann constant, μ is the thermodynamic activity and T is the temperature (Sato, 1993).

The dimorphic polymorph which exhibits the lowest activation energy barrier and highest pre-exponential frequency term will therefore demonstrate the highest nucleation rate allowing preferential polymorphic crystallization (Rodriguez-Hornedo and Murphy, 1999). The size of the kinetic barrier decreases with supersaturation (Bernstein et al., 1999) and supersaturation is always greater for SX I than SX II below the transition temperature. The latter kinetic-thermodynamic balance supports the suggestion that the most stable form in a dimorphic system can crystallize under all conditions (Threlfall, 2000).

Seeds of SX form II must be present in order for re-crystallization of the SX II from the melt (Tong et al., 2001, 2003). PEG-crystallized SX I was shown to be free of such seeds by hot stage microscopy (Fig. 7). The thermal behaviour revealed material crystallized from PEG solvents to undergo significantly and substantially lower conversion to SX II (i.e. SX PEG 400B) or no conversion at all. The thermal behaviour of SX PEG 6000 demonstrated that homogeneous nucleation of SX II from the melt was not favoured kinetically. The assumption that the SEDS form I material is free from SX II seeds (Tong et al., 2001, 2003) is to be questioned because although their presence was undetected by PXRD, re-crystallization from the melt was observed.

The solid–solid transition (i.e. not involving melt re-crystallization) of SX I into SX II for milled SX PEG 6000 was consistent with enantiotropic polymorphism (Burger and Ramberger, 1979) where transformation occurs above the transition temperature upon heating (Dunitz, 1995). It is not unknown for milling to induce polymorphic transition directly in enantiotropic systems (Brittain, 2002; Chikhalia et al., 2006). Thus seeds of SX II may have been created as a result of the milling process *per se*, as suggested by Tong et al. (2003). Such seeds represent a microphase undetectable by PXRD (Shekunov et al., 2002). Disorder introduced into SX PEG 6000 following milling was associated with solid-state transformation and facilitation of re-crystallization from the SX I melt.

An alternative hypothesis is that seeds of SX II only form upon heating above the enantiotropic transition temperature due to the presence of regions of milling-induced short-range disorder (e.g. lattice strain, point dislocations). Crystals of a low temperature phase that are substantially free from defects resist solid-state transformation, and thus melt at the fusion point of that polymorph (Dunitz, 1995). However, highly localized solid-state transformation can occur at short-range defects under thermal or mechanical stress (Morris et al., 2001) which create the SX II seeds present upon melting of the predominant polymorph, SX I. Indeed SX crystallized from propan-2-ol possesses higher strain and smaller crystalline domains than SEDS SX I (Shekunov et al., 2002; Tong et al., 2002).

Table 4
The thermal behaviour indicating the onset and peak temperatures of transition (or melting) of SX form I polymorph ($T_{t/m}$ and T_p), the enthalpy of polymorphic transition (ΔH_t), the onset temperature of melting (T_m) and the enthalpy of fusion (ΔH_f) of the SX form II polymorph at varying heating rates (β) (mean ± S.D., $n \geq 3$)

	β (°C min^{-1})				
	2	5	10[a]	20[a]	70[a]
$T_{t/m}$ (°C)	111.4 ± 1.4	110.7 ± 1.4	114.5 ± 0.5	116.2 ± 0.2	116.1 ± 0.6
T_p (°C)	115.1 ± 1.1	115.4 ± 1.3	119.5 ± 0.5	121.5 ± 0.5	121.9 ± 0.3
ΔH_t (kJ mol^{-1})	25.20 ± 0.38	27.96 ± 2.73	–	–	–
T_m SX II (°C)	134.8 ± 1.3	133.1 ± 1.2	136.7 ± 0.5	136.2 ± 0.9	136.1 ± 1.1
ΔH_f SX II (kJ mol^{-1})	44.41 ± 0.80	43.26 ± 0.94	44.02 ± 5.78	41.90 ± 0.36	15.66 ± 0.43

[a] The polymorphic transition merged with the melting of the SX I polymorph at these heating rates.

Short-range disorder in the lattice resulting from crystallization may be exaggerated upon milling (Byard et al., 2005). Thus, heterogenous re-crystallization of SX II from the melt results when SX II seeds are created by one of two possible means: upon passing the transition temperature or due to micronization-induced solid-state transition.

5. Conclusions

Microparticles of SX produced by antisolvent crystallization from PEG solvents were crystalline in nature. The microcrystals were of the (low temperature) stable form I polymorph. The absence of re-crystallization of the high temperature polymorph, SX II, upon heating was consistent with a low degree of crystal lattice disorder and with enantiotropic purity. It appeared that re-crystallization of SX II required embryonic seeds of SX II to be present at the melting point of the low temperature polymorph, SX I. The thermo-kinetic behaviour of PEG-crystallized SX pointed to polymorphic control of SX for inhalation formulation when compared to the conventionally micronized material, which exhibited disruption in crystallinity.

The origin of SX II seeds at fusion of SX I remains obscure due to the high limits of detection of PXRD. We conclude that SX II seeds are most likely formed by heat-induced solid-state transformation at localized high-energy lattice defects upon passing the enantiotropic transition temperature (90–110 °C). Such localized disorder can be created during or be increased by milling. Regardless of the origin of SX II seeds, SX crystallized from PEG according to the process of Amphiphilic Crystallization demonstrated higher polymorphic purity and/or fewer crystalline defects than all test and other reported samples. Microparticles suitable for inhalation were therefore produced without inducing solid-state disorder.

Acknowledgements

The authors are grateful to King's College London and MedPharm Ltd. for financial support of this work and to Prof. Peter York for providing SEDS salmeterol.

References

Avrami, M., 1939. Kinetics of phase change I—general theory. J. Chem. Phys. 7, 1103–1112.
Avrami, M., 1940. Kinetics of phase change. II. Transformation-time relations for random distribution of nuclei. J. Chem. Phys. 8, 212–224.
Avrami, M., 1941. Granulation, phase change, and microstructure—kinetics of phase change III. J. Chem. Phys. 9, 177–184.
Beach, S., Latham, D., Sidgwick, C., Hanna, M., York, P., 1999. Control of the physical form of salmeterol xinofoate. Org. Process Res. Dev. 3, 370–376.
Bernstein, J., Davey, R.J., Henck, J.O., 1999. Concomitant polymorphs. Angew. Chem. 38, 3440–3461.
Blagden, N., Davey, R.J., 2003. Polymorph selection: challenges for the future? Cryst. Growth Des. 3, 873–885.
Brittain, H.G., 2002. Effects of mechanical processing on phase composition. J. Pharm. Sci. 91, 1573–1580.
Burger, A., Ramberger, R., 1979. Polymorphism of pharmaceuticals and other molecular-crystals. 1. Theory of thermodynamic rules. Mikrochim. Acta 2, 259–271.
Byard, S.J., Jackson, S.L., Smail, A., Bauer, M., Apperley, D.C., 2005. Studies on the crystallinity of a pharmaceutical development drug substance. J. Pharm. Sci. 94, 1321–1335.
Chikhalia, V., Forbes, R.T., Storey, R.A., Ticehurst, M., 2006. The effect of crystal morphology and mill type on milling induced crystal disorder. Eur. J. Pharm. Sci. 27, 19–26.
Chung, K.F., O'Byrne, P.M., 2003. Pharmacological agents used to treat asthma. Eur. Respir. Monogr., 339–375.
Dunitz, J., 1995. Phase changes and chemical reactions in molecular crystals. Acta Crystallogr. B 51, 619–631.
Elamin, A.A., Ahlneck, C., Alderborn, G., Nystrom, C., 1994. Increased metastable solubility of milled griseofulvin, depending on the formation of a disordered surface structure. Int. J. Pharm. 111, 159–170.
Giacovazzo, C., 1996. Direct methods and powder data: state of the art and perspectives. Acta Crystallogr. A 52, 331–339.
Heng, J.Y.Y., Thielmann, F., Williams, D.R., 2006. The effects of milling on the surface properties of form I paracetamol crystals. Pharm. Res. 23, 1918–1927.
Kaschiev, D., 2000. Nucleation: Basic Theory with Applications, 1st ed. Butterworth-Heinemann, Oxford.
Langford, J.I., Louer, D., 1996. Powder diffraction. Rep. Progress Phys. 59, 131–234.
Mackin, L., Sartnurak, S., Thomas, I., Moore, S., 2002a. The impact of low levels of amorphous material (<5%) on the blending characteristics of a direct compression formulation. Int. J. Pharm. 231, 213–226.
Mackin, L., Zanon, R., Park, J.M., Foster, K., Opalenik, H., Demonte, M., 2002b. Quantification of low levels (<10%) of amorphous content in micronised active batches using dynamic vapour sorption and isothermal microcalorimetry. Int. J. Pharm. 231, 227–236.
Michaelsen, C., Dahms, M., 1996. On the determination of nucleation and growth kinetics by calorimetry. Thermochim. Acta 288, 9–27.
Morris, K.R., Griesser, U.J., Eckhardt, C.J., Stowell, J.G., 2001. Theoretical approaches to physical transformations of active pharmaceutical ingredients during manufacturing processes. Adv. Drug Del. Rev. 48, 91–114.
Murnane, D., Marriott, C., Martin, G.P., 2008a. Comparison of salmeterol xinafoate microparticle production by conventional and novel antisolvent crystallization. Eur. J. Pharm. Biopharm. 69, 94–105.
Murnane, D., Martin, G.P., Marriott, C., 2008b. Developing an environmentally benign process for the production of microparticles: amphiphilic crystallization. Eur. J. Pharm. Biopharm. 69, 72–82.
Planinsek, O., Buckton, G., 2003. Inverse gas chromatography: considerations about appropriate use for amorphous and crystalline powders. J. Pharm. Sci. 92, 1286–1294.
Pritchard, J.N., 2001. The influence of lung deposition on clinical response. J. Aerosol Med. 14, S19–S26.
Rehman, M., Shekunov, B.Y., York, P., Lechuga-Ballesteros, D., Miller, D.P., Tan, T., Colthorpe, P., 2004. Optimisation of powders for pulmonary delivery using supercritical fluid technology. Eur. J. Pharm. Sci. 22, 1–17.
Rodriguez-Hornedo, N., Murphy, D., 1999. Significance of controlling crystallization mechanisms and kinetics in pharmaceutical systems. J. Pharm. Sci. 88, 651–660.
Sato, K., 1993. Polymorphic transformations in crystal-growth. J. Phys. D: Appl. Phys. 26, B77–B84.
Shah, B., Kakumanu, V.K., Bansal, A.K., 2006. Analytical techniques for quantification of amorphous/crystalline phases in pharmaceutical solids. J. Pharm. Sci. 95, 1641–1665.
Shekunov, B.Y., Feeley, J.C., Chow, A.H.L., Tong, H.H.Y., York, P., 2002. Physical properties of supercritically-processed and micronised powders for respiratory drug delivery. "KONA" Powder Sci. Technol. Jpn., 178–187.
Shekunov, B.Y., York, P., 2000. Crystallization processes in pharmaceutical technology and drug delivery design. J. Cryst. Growth 211, 122–136.
Sonnergaard, J.M., 2006. On the misinterpretation of the correlation coefficient in pharmaceutical sciences. Int. J. Pharm. 321, 12–17.
Steckel, H., Rasenack, N., Villax, P., Muller, B.W., 2003. In vitro characterization of jet-milled and in-situ-micronized fluticasone-17-propionate. Int. J. Pharm. 258, 65–75.
ter Horst, J.H., Kramer, H.J.M., Jansens, P.J., 2002. A new molecular modeling approach to predict concomitant nucleation of polymorphs. Cryst. Growth Des. 2, 351–356.
Threlfall, T., 2000. Crystallisation of polymorphs: thermodynamic insight into the role of solvent. Org. Process Res. Dev. 4, 384–390.
Tong, H.H., Shekunov, B.Y., York, P., Chow, A.H., 2001. Characterization of two polymorphs of salmeterol xinafoate crystallized from supercritical fluids. Pharm. Res. 18, 852–858.
Tong, H.H.Y., Shekunov, B.Y., York, P., Chow, A.H.L., 2002. Influence of polymorphism on the surface energetics of salmeterol xinafoate crystallized from supercritical fluids. Pharm. Res. 19, 640–648.
Tong, H.H.Y., Shekunov, B.Y., York, P., Chow, A.H.L., 2003. Thermal analysis of trace levels of polymorphic impurity in salmeterol xinafoate samples. Pharm. Res. 20, 1423–1429.
Tong, H.H.Y., Shekunov, B.Y., York, P., Chow, A.H.L., 2006. Predicting the aerosol performance of dry powder inhalation formulations by interparticulate interaction analysis using inverse gas chromatography. J. Pharm. Sci. 95, 228–233.
Vazquez, J., Lopez-Alemany, P.L., Villares, P., Jimenez-Garay, R., 2000. Generalization of the Avrami equation for the analysis of non-isothermal transformation kinetics. Application to the crystallization of the $Cu_{0.20}As_{0.30}Se_{0.50}$ alloy. J. Phys. Chem. Solids 61, 493–500.
Vyazovkin, S., Wight, C.A., 1997. Kinetics in solids. Annu. Rev. Phys. Chem. 48, 125–149.
Ward, G.H., Schultz, R.K., 1995. Process-induced crystallinity changes in albuterol sulfate and its effect on powder physical stability. Pharm. Res. 12, 773–779.
York, P., Ticehurst, M.D., Osborn, J.C., Roberts, R.J., Rowe, R.C., 1998. Characterisation of the surface energetics of milled dl-propranolol hydrochloride using inverse gas chromatography and molecular modelling. Int. J. Pharm. 174, 179–186.
Zhang, G.G.Z., Law, D., Schmitt, E.A., Qiu, Y., 2004. Phase transformation considerations during process development and manufacture of solid oral dosage forms. Adv. Drug Del. Rev. 56, 371–390.
Zhou, D.L., Schmitt, E.A., Zhang, G.G., Law, D., Vyazovkin, S., Wight, C.A., Grant, D.J.W., 2003. Crystallization kinetics of amorphous nifedipine studied by model-fitting and model-free approaches. J. Pharm. Sci. 92, 1779–1792.